April 1, 2015

Surface oxidation energetics and kinetics on MoS2 monolayer

Santosh KC, *The University of Texas at Dallas*
Roberto C. Longo, *The University of Texas at Dallas*
Robert M. Wallace, *University of Texas at Dallas*
Kyeongjae Cho, *The University of Texas at Dallas*

Journal of Applied Physics

Surface oxidation energetics and kinetics on MoS_2 monolayer

Cite as: J. Appl. Phys. **117**, 135301 (2015); https://doi.org/10.1063/1.4916536
Submitted: 24 January 2015 . Accepted: 18 March 2015 . Published Online: 01 April 2015

Santosh KC, Roberto C. Longo, Robert M. Wallace, and Kyeongjae Cho

Surface oxidation energetics and kinetics on MoS_2 monolayer

Santosh KC,[1] Roberto C. Longo,[1] Robert M. Wallace,[1,2] and Kyeongjae Cho[1,2,a)]
[1]*Department of Materials Science & Engineering, The University of Texas at Dallas, Richardson, Texas 75080, USA*
[2]*Department of Physics, The University of Texas at Dallas, Richardson, Texas 75080, USA*

(Received 24 January 2015; accepted 18 March 2015; published online 1 April 2015)

In this work, surface oxidation of monolayer MoS_2 (one of the representative semiconductors in transition-metal dichalcogenides) has been investigated using density functional theory method. Oxygen interaction with MoS_2 shows that, thermodynamically, the surface tends to be oxidized. However, the dissociative absorption of molecular oxygen on the MoS_2 surface is kinetically limited due to the large energy barrier at low temperature. This finding elucidates the air stability of MoS_2 surface in the atmosphere. Furthermore, the presence of defects significantly alters the surface stability and adsorption mechanisms. The electronic properties of the oxidized surface have been examined as a function of oxygen adsorption and coverage as well as substitutional impurities. Our results on energetics and kinetics of oxygen interaction with the MoS_2 monolayer are useful for the understanding of surface oxidation, air stability, and electronic properties of transition-metal dichalcogenides at the atomic scale. © *2015 AIP Publishing LLC*.
[http://dx.doi.org/10.1063/1.4916536]

I. INTRODUCTION

Recently, transition-metal dichalcogenides (TMDs) have attracted huge research interest[1–3] of the scientific community because of their unique features and tunability of their electronic, optical, and tribological properties, which open possibilities of diverse applications.[4–13] Molybdenum disulphide (MoS_2) is one of the TMDs that have been successfully exfoliated using various techniques into a very stable single monolayer or few layers thick material.[14–20] Each layer consists of two hexagonal planes of S atoms and a hexagonal plane of Mo atoms coordinated through covalent interactions with the S atoms in a trigonal prismatic coordination. Thus, the S–Mo–S intra-layer stack is tightly bound, whereas S–Mo–S—S–Mo–S interlayers are held together by weakly interacting van der Waals forces. Monolayer MoS_2 has a direct band gap of 1.8 eV (Refs. 21–23) and it has been recently investigated for low-power field effect transistors, showing promising performance of high on/off current ratio (10^8) and a carrier mobility $\sim$200 cm^2/Vs with a high-κ gate dielectric.[1,2]

Apart from the recent realization of MoS_2 in electronic device applications, it has also been used as solid lubricant[24,25] in spacecraft. The environmental effects of low earth orbit on the friction coefficient and wear-life have been studied, which will determine the useful life of a satellite system under atomic oxygen beam exposures. Depending on the concentration of atomic oxygen, the frictional coefficients might be decreased, hampering the lubricating properties. The effect of oxidation on the wear-life of MoS_2 films has also been reported.[25] Surface oxidation affects the electronic, optical, and tribological properties of MoS_2. Therefore, a detailed and quantitative understanding of the oxidation process, based on the atomic structures and electronic properties, would help the fabrication process of electronic devices, including finding suitable passivation techniques. The oxidation energies at edge sites of MoS_2 nanoparticles with different terminations and S coverage have been reported,[26] and the physisorption of various gases on TMD has also been studied.[27] However, the atomic level details of the chemisorption, oxidation mechanisms, together with their energetics and kinetics, have not been explored yet, which is an essential requirement in order to successfully realize TMD-based devices.

In this work, atomic and molecular oxygen (O_2) interaction with the MoS_2 surface and their corresponding electronic properties using density functional theory (DFT) calculations are presented. The impact of defective MoS_2 surface on the adsorption kinetics and the corresponding electronic properties is also reported.

II. COMPUTATIONAL METHOD

Theoretical calculations based on DFT,[28,29] with plane wave basis sets and Projector Augmented Wave (PAW) pseudopotentials implemented in the Vienna *Ab initio* Simulation Package (VASP)[30,31] have been carried out. The electronic wave functions are represented by plane wave basis with a cutoff energy of 500 eV. The accuracy of the DFT results depends on the exchange-correlation functional used. Since the local density approximation (LDA) is found to overestimate the binding energy,[32,33] the exchange correlation interactions are incorporated as a functional of the Generalized Gradient Approximation (GGA)[34–36] in the present work. To investigate the surface oxidation, a monolayer of 5×5 supercell (15.8 Å $\times$ 15.8 Å) of MoS_2 surface model is used (see Figs. 1 and 2(a)). This surface model contains two atomic layers of S and one atomic layer of Mo, which are periodically repeated. Each periodic layer is separated by 16 Å of vacuum to avoid interaction between the

a)Author to whom correspondence should be addressed. Electronic mail: kjcho@utdallas.edu

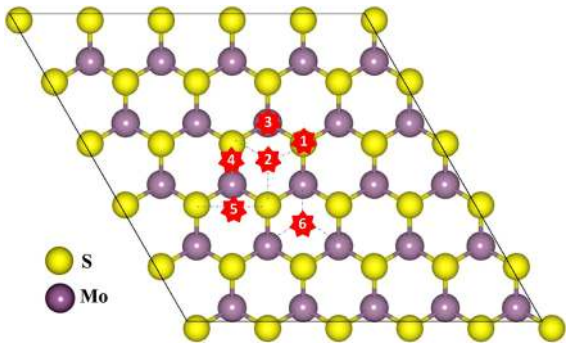

FIG. 1. All the possible sites for O adsorption considered in this work: (1) On top of S atom (S-O), (2) hallow top space (S-O-S), (3) on top of Mo atom (Mo-O), (4) Mo-S bridge site (Mo-O-S), (5) S-O-S top bridge (S-O-S top), and (6) hallow top space (Mo-O-Mo).

two surfaces of the layer and their replica images. A gamma centered $6 \times 6 \times 1$ k-point mesh is employed in the self-consistent field (SCF) calculations and a $12 \times 12 \times 1$ k-point mesh is employed for density of states (DOSs) calculations. First, the pristine surface was fully relaxed and, for subsequent calculations of the oxidation effects, the volume of the supercell size was kept fixed, whereas atomic positions were allowed to relax. The energy and Hellmann-Feynman force convergence criteria are 10^{-4} eV and 0.01 eV/Å, respectively. The nudged elastic band (NEB) method[37–40] is used to investigate the oxygen absorption and diffusion kinetics, and to estimate the corresponding adsorption energy barrier on both pristine and defective MoS_2 surfaces.

III. RESULTS AND DISCUSSION

A. MoS_2 (001) surface exposure to atomic and molecular oxygen

First of all, in order to investigate the interaction of atomic O with the MoS_2 surface, various configurations are generated and optimized and, then, we compare their thermodynamic relative stability. Figure 1 shows the various possible O adsorption sites, labeled as: (1) On top of S atom (S-O), (2) hallow top space (S-O-S), (3) on top of Mo atom (Mo-O), (4) Mo-S bridge site (Mo-O-S), (5) S-O-S top bridge (S-O-S top), and (6) hallow top space (Mo-O-Mo). The O adsorption energies on various sites confirmed that the most favorable O adsorption site (labeled (1) in Fig. 1) is on top of a S atom, with S-O bond length of 1.487 Å and adsorption energy of ≈ -1.12 eV, as shown in Fig. 2(b). O adsorption at sites 2 and 5 transformed into site 1 after relaxation. O adsorption on metal (site 3) has positive formation energy of 0.94 eV with respect to pristine surface. Also, sites 4 and 6 have positive formation energies of 0.95 eV and 0.25 eV higher than the pristine surface. Upon adsorption on the surface, the O slightly displaces the sulfur atom downwards, resulting in S-Mo bond lengths of 2.384 Å, as compared to 2.410 Å for the pristine MoS_2 surface.

The impact of O adsorption on the electronic structure of MoS_2 has been investigated by analyzing the DOS, as shown in Fig. 2(d). O adsorption does not introduce gap states. However, the adsorption slightly affects the band edges, showing some peaks in the conduction band (CB) close to the edge. For a single O adatom on a 5×5 MoS_2 supercell (corresponding to a defect concentration of 4.6×10^{13} O atoms/cm^2), there is no appreciable band gap change. There is some interaction of O with S atom, as can be seen in the DOS (see the arrows in Fig. 2(d)). However, the Mo DOS shows no significant change even close to the adsorbed site. This interaction of O with surface S has very important implications on field effect device fabrication, facilitating the functionalization of the MoS_2 surface.[5,41]

To examine the trend in the change of electronic properties and thermodynamical stability, the concentration of adsorbed O is increased from O_1 (4.6×10^{13} O atoms/cm^{-2}

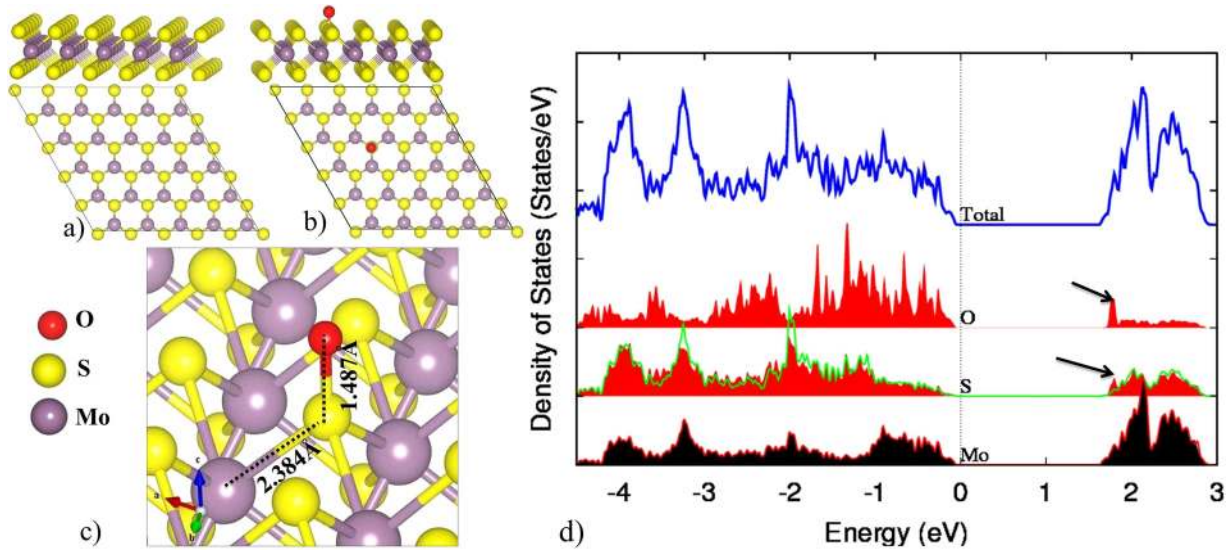

FIG. 2. a) Atomic structure of pristine MoS_2 monolayer (the top figure shows the side view), (b) the most stable configuration for single atomic oxygen adsorption on the pristine MoS_2 monolayer, and (c) zoomed and angled image of the configuration (b), showing the atomic coordination and bond lengths. Oxygen, sulfur, and molybdenum are represented by red, yellow, and purple spheres, respectively. (d) DOS for O adsorption (4.6×10^{13} O atoms/cm^2 or 4% coverage) on a 5×5 MoS_2 monolayer supercell. The blue line corresponds to the total DOS, the green line is the bulk sulphur DOS, and the red line shows bulk Mo DOS, which is overlapped with black filled lines of Mo atoms close to the adsorption site. Arrows show the states introduced in the conduction band due to O adsorption.

TABLE I. Oxygen adsorption energy and electronic band gap variation with O coverage.

No	Configuration	Coverage (Oads) (%)	Coverage (Oads) O atoms/cm^2	E^{form} (ads) (eV)	E^{form} (ads) (eV/#O)	Band gap (eV) GGA
	Pristine	0	0	…	…	1.757
I	O_1	4	4.60×10^{13}	−1.12	−1.12	1.750
II	O_2	8	9.20×10^{13}	−2.15	−1.07	1.727
III	O_3	12	1.38×10^{14}	−3.14	−1.05	1.700
IV	O_4	16	1.84×10^{14}	−4.11	−1.03	1.696
V	O_5	20	2.30×10^{14}	−5.06	−1.01	1.678
VI	O_6	24	2.76×10^{14}	−6.01	−1.00	1.658
VII	O_7	28	3.22×10^{14}	−6.97	−0.99	1.642
VIII	O_{25}	100	1.15×10^{15}	−21.93	−0.87	1.449

or 4% coverage) to O_{25} (equivalent to 1.15×10^{15} O atoms/cm^2 or 100% coverage). The thermodynamic stability of the O adsorbed surfaces is characterized by their formation energies, obtained using the following equation:

$$E^{form}(ads) = E(ads) - E(pristine) - n\mu_O, \qquad (1)$$

where E^{form} (*ads*) is the formation energy of oxidized surface of MoS_2 with total DFT energy E (*ads*), E (*pristine*) is the DFT energy of the clean surface, and μ_O is the reference chemical potential of O adsorbed species with n number of atoms. The computed value of μ_O is −4.36 eV per atom, as obtained from gas phase O_2 molecule. Negative (positive) values of the formation energy indicate that the surface, thermodynamically, favors (does not favor) oxidation. The adsorption energies and the corresponding electronic band gaps of MoS_2 with oxidized surfaces are listed in Table I, where O_x represents the adsorption of x number of O atoms on a 5×5 MoS_2 supercell. O_1 is equivalent to a concentration of 4.6×10^{13} O atoms/cm^2 (4% coverage), whereas O_{25} is equivalent to 1.15×10^{15} O atoms/cm^2 (100% coverage).

Table I shows that the O adsorption energies are always negative, compared to the pristine surface, indicating that the surface has a tendency to be oxidized and the stability of the adsorbed O species depends on their coverage. The more O atoms adsorbed on the surface, the lesser their relative stability due to adsorbate interaction, as can be seen in the formation energy per O atom in Table I. However, as will be discussed later, the kinetics of the adsorption will provide accurate information on the likelihood of this process at a given temperature. The band gap changes with the O adsorption, as can see in Fig. 3, which shows the DOS as a function of O coverage.

Figure 3 shows that the band gap narrows down as the O coverage increases: the band gap is changed by 0.3 eV for the full coverage of O adsorption with respect to the pristine MoS_2. This result indicates that the O adsorption does not introduce deep gap states in the fundamental band gap of MoS_2. The O-introduced states lie in the conduction band edge, as shallow states contributing to the gap narrowing. For a low O coverage (below 10%, O_1, O_2), the change in the band gap is insignificant as compared with higher O concentration. This is due to the small change in the hybridization of S p and Mo d orbitals because of the additional O atoms. For larger O coverages, the band gap change is more noticeable. However, this high concentration of surface O may be very reactive, and they could damage the MoS_2 surface producing, at the same time, some desorption of the O species evolving into O_2 molecules or Mo-S bond scission evolving into S-O_x species as well as Mo-O bond formation, depending on their respective reaction kinetics.

The thermodynamic stability of the O adsorption is further investigated by studying the formation energy with respect to the oxygen chemical potential at different temperature and pressure, in order to simulate experimental conditions. The relative formation energy as a function of the oxygen chemical potential and oxygen partial pressure at 600 K is shown in Fig. 4. The total DFT energies are used instead of the Gibbs free energies for the calculations of the formation energies because the entropy contributions and enthalpy changes due to finite temperatures (300–600 K) are negligible for all of the structures considered, resulting in no significant changes in the relative formation energies. The following equation to correlate the chemical potential with oxygen partial pressure has been used:[42,43]

$$\mu_0(T,P) = \mu_0(T,P^0) + \frac{1}{2}kT\ln\left(\frac{P}{P^0}\right), \qquad (2)$$

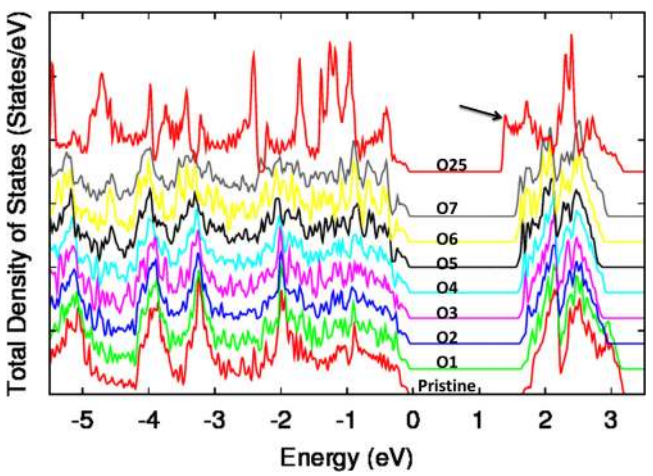

FIG. 3. Total DOS for various O adsorption coverages: from O_1 (4.6×10^{13} O atoms/cm^2, corresponding to 4% coverage) to O_{25} (1.15×10^{15} O atoms/cm^2 or full coverage) on a 5×5 supercell of MoS_2 monolayer. The arrow shows the additional conduction band states introduced in the band gap for high O adatom coverage.

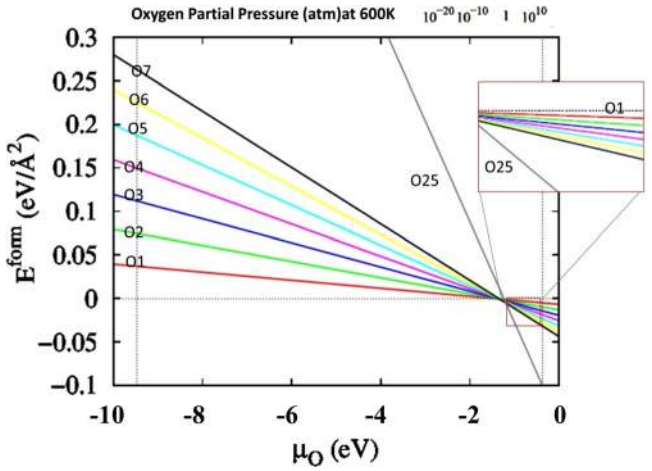

FIG. 4. Surface formation energy of O adsorption in MoS_2 monolayer. The zoomed inset shows the experimentally realistic region of oxygen chemical potential. The range of chemical potential is obtained by considering oxygen rich to oxygen poor conditions. The zero of the energy (y-axis) corresponds to the pristine surface.

where p and p^O are the partial pressures at temperature T and at one atmosphere, respectively.

The whole range of thermodynamically allowed O chemical potential is labeled in the lower x-axis (see Fig. 4), and the corresponding oxygen partial pressure is labeled in the upper x-axis. The thermodynamically allowed chemical potential range is estimated until the formation of SO_2. Thus, only a small portion of the plot corresponds to realistic MoS_2 oxidation experimental conditions, shown in the zoomed image of Fig. 4, indicating the experimentally achievable environment (close to a partial pressure of 1 atm). The right hand side of the x-axis refers to the O-rich region, whereas the left hand side corresponds to an O-poor environment. We used the gas phase O_2 molecule and SO_2 as reference states, similarly to the formulation explained in previous works.[42,43]

The standard molar enthalpies (heat) of formation ($\Delta_f H°$) at 298.15 K for MoS_2, MoO_2, and MoO_3 are −235.1, −588.9, and −745.1 kJ/mol (−2.436, −6.1035, and −7.7224 eV), respectively.[44] Their relative stability can be predicted by comparing the heat of formation of these materials from their constituents. The data show that MoO_x are thermodynamically stable species, consistent with our findings. However, it is very important to study the O_2 dissociative adsorption kinetics, which to a large extent will determine the O_2 adsorption and desorption process in the atmosphere. Figure 4 shows that, thermodynamically, adsorption of atomic O is favorable at oxygen rich environment. In this region, the formation energy is lowered with the increase of adsorbed O concentration, indicating the tendency of the MoS_2 surface to be oxidized.

B. Oxygen as substitutional impurities on MoS_2 surface

After investigating the O adsorption on the MoS_2 surface, the adsorbed O as substitutional impurities, replacing surface sulphur atoms, were also studied. Several configurations with different concentrations of O atoms replacing surface S atoms were investigated. They are labeled as O_x, where x represents the number of O atoms replacing surface S atoms. The substitutional energy for a single S replaced by O (4.6×10^{13} O atoms/cm^2) is ≈−1.91 eV, with respect to the pristine MoS_2 surface. The Mo-O bond lengths and atomic co-ordinations are shown in Figs. 5(a) and 5(b). The atomic position of O is shifted down by ≈0.541 Å relative to the top S position, resulting in three Mo-O bonds with a length of 2.072 Å for each one.

The results show that, thermodynamically, it is favorable to fill S vacancies with substitutional O atoms, although the kinetics of this process at a given temperature still needs to be investigated. Table II shows the impact of substitutional O atoms occupying the surface S sites as a function of the O coverage. The band gaps decrease due to the change in the Mo d orbital and S p orbital hybridization at valence band maximum (VBM) due to O p states that introduce a shallow impurity state in the VBM. Thermodynamically, S vacancies are more favorable than Mo vacancies, as reported in the literature.[45,46] Thus, O atoms substituting surface S atoms are more favorable than Mo atoms. Table II lists the formation energies of the substitutional O impurities, obtained with the following equation:

$$E^{form}(Rep) = E\ (Rep) - E\ (pristine) - n\mu_O + n\mu_S, \quad (3)$$

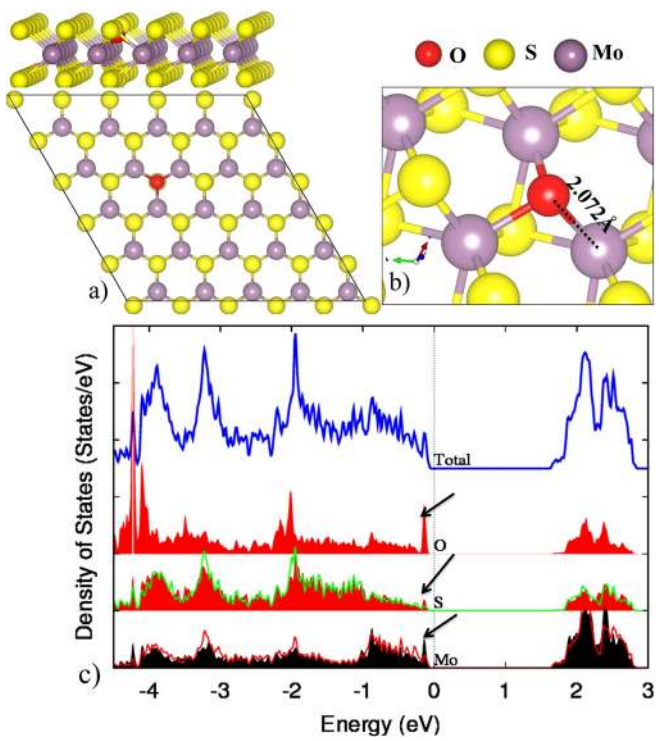

FIG. 5. a) Optimized atomic structure of a MoS_2 monolayer (the top figure shows the side view) configuration containing a single substitutional atomic oxygen replacing a S atom on MoS_2 surface, and (b) the zoomed in configuration with an angled image showing the O atomic coordination and the corresponding bond lengths. Oxygen, sulfur, and molybdenum are represented by red, yellow, and purple spheres, respectively. (c) DOS for substitutional O replacing one surface S atom (4.6×10^{13} O atoms/cm^2 or 4% coverage) on a 5 × 5 supercell of MoS_2 monolayer. The blue line is the total DOS, the green line represents bulk-like sulphur DOS, and, finally, the red line corresponds to bulk Mo DOS. The filled S and Mo DOS represent sites close to the O atom. Arrows show the states in the valance band edge of MoS_2.

TABLE II. Formation energy of substitutional O atoms replacing surface S atoms and their corresponding band gap variation as a function of the O coverage.

No	Configuration	Coverage (Rep) (%)	Coverage (Rep) O atoms/cm^2	E^{form} (Rep) (eV)	E^{form} (Rep) (eV/#O)	Band gap (eV) GGA
	Pristine	0	0	…	…	1.757
I	O_1	4	4.60×10^{13}	−1.912	−1.91	1.742
II	O_2	8	9.20×10^{13}	−3.754	−1.88	1.664
III	O_3	12	1.38×10^{14}	−5.583	−1.86	1.571
IV	O_4	16	1.84×10^{14}	−7.355	−1.84	1.488
V	O_5	20	2.30×10^{14}	−9.084	−1.82	1.403
VI	O_6	24	2.76×10^{14}	−10.767	−1.79	1.320
VII	O_7	28	3.22×10^{14}	−12.471	−1.78	1.242
VIII	O_{25}	100	1.15×10^{15}	−37.640	−1.51	0.264

where E^{form} (*Rep*) is the formation energy of the substitutional O impurity that replaces surface S species of a MoS_2 monolayer with total DFT energy *E* (*Rep*), *E (pristine)* is the DFT energy of the pristine MoS_2 surface, μ_O and μ_S are the reference chemical potentials of O and S, and *n* is the number of substitutional O and/or replaced S atoms. Under this definition, negative values of the formation energy refer to thermodynamically stable substitutional process.

Table II shows that the formation energy is negative with respect to the pristine MoS_2 surface for all the O coverages studied in this work, indicating that O substitutional impurities are always thermodynamically favorable. The formation energy per O substitutional impurity decreases with coverage. For large coverage, this fact indicates that the structural changes induced by O impurities may result in the damage of the MoS_2 surface. In addition, O substitutional impurities significantly change the electronic band gap, as compared to the O adsorption process, because of the nature of the impurity states, as we described previously (cf. Tables I and II).

The total DOS of the substitutional O impurities on the MoS_2 surface for various O concentrations are shown in Fig. 6. As can be seen in the figure, there are impurity states in the band edges, causing the band narrowing due to changes in the metal-chalcogen hybridization strengths. The concentration of impurity states increases with O coverage tending towards metallic character. The MoO_2 structure has been reported to be metallic[47,48] with high chemical stability. With the increase of O coverage and the subsequent formation of Mo-O bonds, the band gaps decrease, thus exhibiting more metallic nature.

Similar to the O adsorption study, we further analyze the formation energy under realistic experimental conditions. The thermodynamically allowable range of oxygen chemical potential is obtained taking into account the extreme cases of oxidation (forming MoO_x) and no oxidation. The right hand side of x axis (Fig. 7) corresponds to O rich environment obtained from gas phase O_2 and the far left side refers to an oxygen deficient environment, obtained from the heat of formation of MoO_2.

Figure 7 shows the relative surface formation energy for O substitutional impurities on the MoS_2 monolayer. The results show that O substitutional impurities are also thermodynamically favorable with respect to the MoS_2 pristine surface. However, an O_2 dissociation kinetics is necessary to confirm the likelihood of O diffusion in order to form Mo-O bonds. It shows that the reactivity of TMDs is different than the well-studied 2D surface of graphene, which is less

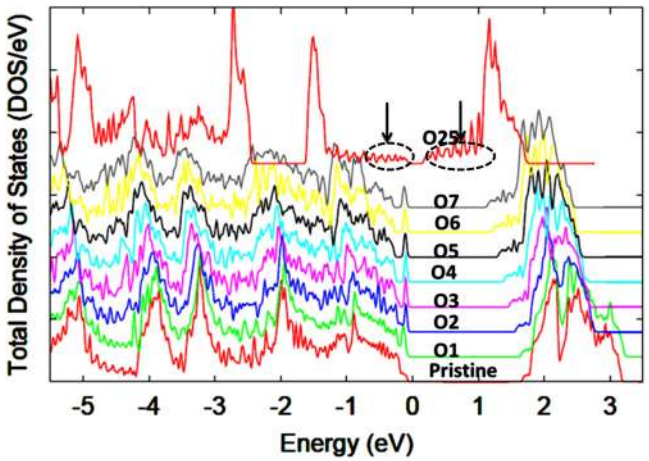

FIG. 6. Total DOS of substitutional O impurities in MoS_2 surfaces, as a function of the O coverage: from O_1 (4.6×10^{13} O atoms/cm^2 or 4% coverage) to O_{25} (1.15×10^{15} O atoms/cm^2 or full coverage) on a 5 × 5 supercell of MoS_2 monolayer. The arrows in the plot show the gap states introduced due to high oxygen coverage.

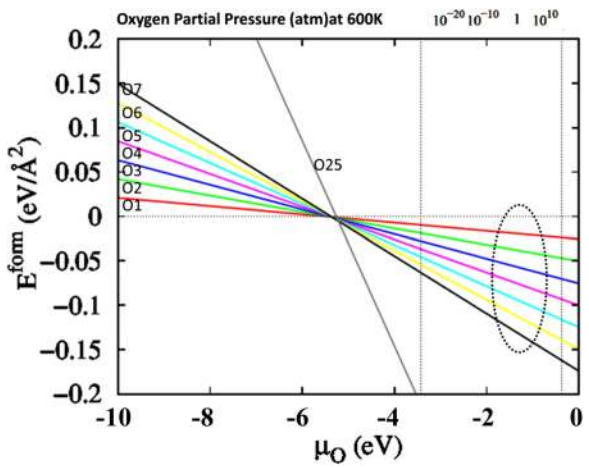

FIG. 7. Surface formation energy of substitutional O in MoS_2 monolayer. The circled part shows the region of realistic experimental conditions of oxygen chemical potential close to 1 atm partial pressure of oxygen. The zero of the energy (y-axis) corresponds to the pristine surface.

susceptible to oxidation, according to several published reports.[49,50]

In addition, the result of the combined O substitutional and adsorbed processes and the impact on the electronic structure of the MoS_2 monolayer is investigated. Figure 8(a) shows the atomic structure of substitutional and adsorbed O atoms on a MoS_2 monolayer. At low concentrations (below 8%), both type of defects do not alter the electronic properties significantly, as can be seen in the local DOS shown in Fig. 8(b). Large concentration of those substitutional and adsorbed species will damage the MoS_2 surface due to surface reaction evolving SO_x species. This may arise as a result of oxygen or ozone treatment of the surface which has been referred to as the ozone functionalization of the MoS_2,[41] since ozone supplies O adatoms. The oxygen atoms adsorbed on top of S and O atom passivating the S vacancy do not interact significantly; only small changes in the DOS can be then noticed, resulting in a superposition of the DOS shown in Figs. 1(d) and 2(c).

Sulphur vacancies introduce defect states close to the conduction band minimum (≈0.6 eV below CBM),[46] which are then removed by the O atoms that occupy the S vacant site. This defect passivating mechanism could play an important role in obtaining a good quality oxide interface with the corresponding dielectric material. This effect might also have some impact on the nature of the interface including enhanced electrical properties of MoS_2 in contact with a high-κ dielectric oxide.[1,51,52]

TMD oxidation has been poorly understood so far as compared with other semiconductor materials. The silicon surface shows a high affinity for oxygen adsorption and, thus, forms an oxide layer rapidly upon exposure to the atmosphere, which helps in the device fabrication process, creating high quality interfaces[53] after thermal treatment, enabling passivation of possible surface defects, and dielectric isolation.[54–58] In case of III–V based semiconductors, the native oxides have been responsible for the poor interface quality of metal-oxide-semiconductor (MOS) devices. This leads to the emphasis on surface preparation and control of oxidation and passivation mechanism.[58,59] The unique structural, chemical, and electronic nature of TMDs surfaces makes the oxidation process quite different from group IV, III–V, or graphene-based semiconductor materials.[49,59–61]

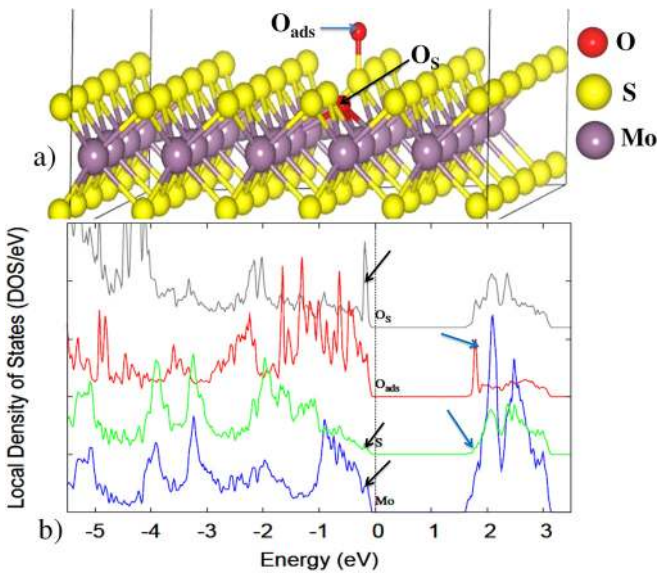

FIG. 8. (a) Atomic positions of substitutional and adsorbed O atoms on MoS_2 surface as indicated by arrows, and (b) local DOS of selected atoms (O_s, O_{ads}, bulk S and bulk Mo atoms). The arrows on DOS point out the additional states introduced as a result of O adsorption and replacement.

C. Oxygen adsorption kinetics on pure and defective MoS_2 monolayer

After studying the thermodynamical stability of the MoS_2 monolayer upon oxygen adsorption, in order to further clarify the oxidation mechanism, the kinetic barrier for the oxygen dissociative adsorption process is obtained. First, a defect-free MoS_2 surface is used to investigate the kinetic energy barrier for the dissociative adsorption of molecular oxygen. Several pathways have been considered in our study, and the investigation on the most favorable pathway is discussed. The initial and final configurations are shown in Fig. 9(a) along with the barrier energy. The kinetic energy barrier is ≈1.59 eV, relatively high, which indicates that the MoS_2 surface is chemically stable in the atmosphere at low temperatures. However, in the presence of a sulphur vacancy defect on the surface, oxygen adsorption and subsequent dissociation kinetic barrier are reduced by half (≈0.8 eV), which indicates that the S vacancy can be easily passivated with molecular oxygen. This finding shows that when S deficient MoS_2 surface is exposed to the atmosphere, it will readily be filled by oxygen. Furthermore, as shown in Fig. 8(b) for lower concentration, O_s does not change the electronic properties significantly. These results highlight that defect sites on the surface exhibit high reactivity. Vacancy sites are responsible for catalytic activities and oxygen chemisorption in MoS_2, since metal (Mo) sites are partially or completely exposed to the atmosphere due to S vacancies depending on their defect concentration.

Therefore, our results have clarified that the main reason for the air stability of MoS_2 surface is the high kinetic energy barrier for the adsorption of molecular oxygen, even though

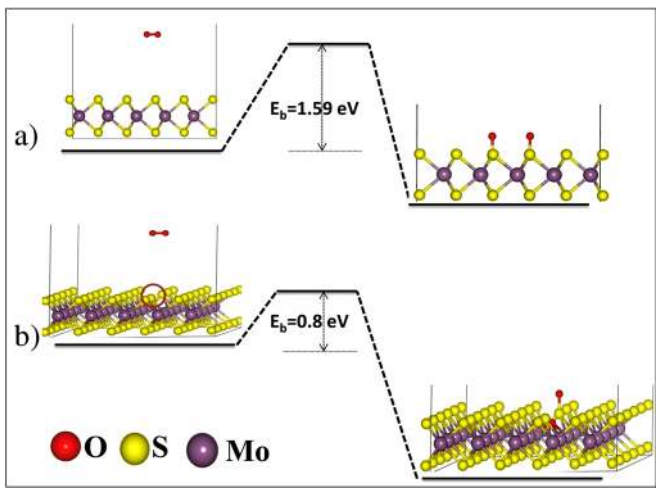

FIG. 9. Oxygen dissociative adsorption barrier on (a) pristine MoS_2 surface and (b) S deficient MoS_2 surface.

the adsorbed atomic oxygen is thermodynamically stable on the MoS_2 surface. Our findings also indicate that S defects on the MoS_2 surface can act as reactive centers for O_2 dissociation and adsorption. This result points an important implication for the properties of TMD-based semiconductor devices. Moreover, adsorption reactivity of TMDs can be affected by the substrate, as was shown for hydrogen adsorption by MoS_2 on transitional metal substrates.[62] A similar approach can be extended to other species like OH, H_2O, in order to investigate the comparative analysis of TMDs air stabilities, which will be discussed in a separate article in the future.

IV. SUMMARY

DFT-based calculations have been performed in order to investigate the surface oxidation mechanisms of monolayer MoS_2 using both atomic and molecular oxygen. Our results indicate that O adsorption on MoS_2 surface is thermodynamically favorable. Moreover, at low concentrations, O adatoms do not alter the band gap significantly. In addition, oxygen substitutional impurities on a S-vacancy of MoS_2 surface are thermodynamically favorable as well. Oxygen is able to passivate any sulphur vacancy produced as a result of the exfoliation process, because of its isoelectronic nature. However, the MoS_2 electronic band gap is reduced significantly with increasing O concentration causing a significant change in the strength of Mo-S orbital hybridization at the valence band edge. When simultaneous adsorption and oxygen substitutional impurities are present on the MoS_2 surface, there is also no significant impact on the electronic properties at very low oxygen concentrations, except some impurity states close to both band edges. An O_2 absorption kinetics study reveals that pristine MoS_2 surface oxidation is kinetically limited due to the large oxygen dissociative adsorption barrier, even though the oxygen is thermodynamically stable when adsorbed on the MoS_2 surface. However, on a S deficient MoS_2 surface, the kinetic energy barrier is substantially lower, indicating that the oxidation process will be both kinetically and thermodynamically favored and the MoS_2 surface easily passivated, both structurally and electronically. This information will then be very useful to understand the surface oxidation, air stability, and electronic properties of TMD-based electronic devices.

ACKNOWLEDGMENTS

We would like to thank the LEAST research group at UTD, in particular, Professor Christopher Hinkle, Dr. Luigi Colombo, Dr. Stephen McDonnell, Dr. Rafik Addou, and Ms. Angelica Azcatl for useful discussions. This work was supported in part by the Center for Low Energy Systems Technology (LEAST), one of six centers supported by the STARnet phase of the Focus Center Research Program (FCRP), a Semiconductor Research Corporation program sponsored by MARCO and DARPA. All the calculations are performed using computational resources of Texas Advanced Computer Center (TACC) at University of Texas at Austin.

[1]B. Radisavljevic, A. Radenovic, J. Brivio, V. Giacometti, and A. Kis, Nat. Nanotechnol. **6**, 147 (2011).
[2]M. Chhowalla, H. S. Shin, G. Eda, L.-J. Li, K. P. Loh, and H. Zhang, Nat. Chem. **5**, 263–275 (2013).
[3]Q. H. Wang, K. Kalantar-Zadeh, A. Kis, J. N. Coleman, and M. S. Strano, Nat. Nanotechnol. **7**, 699–712 (2012).
[4]H. Li *et al.*, Small **8**, 682–686 (2012).
[5]A. Azcatl *et al.*, 2D Mater. **2**, 014004 (2015).
[6]H. Li *et al.*, Small **8**, 63–67 (2012).
[7]A. H. Castro Neto, Phys. Rev. Lett. **86**, 4382–4385 (2001).
[8]A. K. Geim and I. V. Grigorieva, Nature **499**, 419–425 (2013).
[9]M. Fontana, T. Deppe, A. K. Boyd, M. Rinzan, A. Y. Liu, M. Paranjape, and P. Barbara, Sci. Rep. **3**, 1634 (2013).
[10]Z. Yin, H. Li, H. Li, L. Jiang, Y. Shi, Y. Sun, G. Lu, Q. Zhang, X. Chen, and H. Zhang, ACS Nano **6**, 74–80 (2012).
[11]R. S. Sundaram, M. Engel, A. Lombardo, R. Krupke, A. C. Ferrari, P. Avouris, and M. Steiner, Nano Lett. **13**(4), 1416–1421 (2013).
[12]B. Radisavljevic, M. B. Whitwick, and A. Kis, ACS Nano **5**, 9934–9938 (2011).
[13]W. Ho, J. C. Yu, J. Lin, J. Yu, and P. Li, Langmuir **20**, 5865–5869 (2004).
[14]R. A. Gordon, D. Yang, E. D. Crozier, D. T. Jiang, and R. F. Frindt, Phys. Rev. B **65**, 125407 (2002).
[15]V. Nicolosi, M. Chhowalla, M. G. Kanatzidis, M. S. Strano, and J. N. Coleman, Science **340**, 1420 (2013).
[16]X. Huang, Z. Zeng, and H. Zhang, Chem. Soc. Rev. **42**, 1934–1946 (2013).
[17]A. Castellanos-Gomez *et al.*, Nano Lett. **12**, 3187–3192 (2012).
[18]J. N. Coleman *et al.*, Science **331**, 568–571 (2011).
[19]G. Cunningham *et al.*, ACS Nano **6**, 3468–3480 (2012).
[20]G. Eda *et al.*, Nano Lett. **11**, 5111–5116 (2011).
[21]K. F. Mak, C. Lee, J. Hone, J. Shan, and T. F. Heinz, Phys. Rev. Lett. **105**, 136805 (2010).
[22]A. Splendiani *et al.*, Nano Lett. **10**, 1271–1275 (2010).
[23]A. Kuc, N. Zibouche, and T. Heine, Phys. Rev. B **83**, 245213 (2011).
[24]J. R. Lince and J. R. Frantz, Tribol. Lett. **9**, 211–218 (2001).
[25]M. Tagawaa, M. Muromoto, S. Hachiue, K. Yokota, N. Ohmae, K. Matsumoto, and M. Suzuki, Tribol. Lett. **18**, 437–443 (2005).
[26]T. Liang, W. G. Sawyer, S. S. Perry, S. B. Sinnott, and S. R. Phillpot, J. Phys. Chem. C **115**, 10606–10616 (2011).
[27]Q. Yue, Z. Shao, S. Chang, and J. Li, Nanoscale Res. Lett. **8**(1), 425 (2013).
[28]G. Kresse and J. J. Furthmuller, Comput. Mater. Sci. **6**(1), 15–50 (1996).
[29]R. G. Parr and W. Yang, *Density-Functional Theory of Atoms and Molecules* (Oxford University Press, New York, 1989).
[30]W. Kohn and L. J. Sham, Phys. Rev. **140**, A1133 (1965).
[31]G. Kresse and D. Joubert, Phys. Rev. B **59**, 1758 (1999).
[32]A. Van de Walle and G. Ceder, Phys. Rev. B **59**, 14992 (1999).
[33]A. Gross, *Theoretical Surface Science: A Microscopic Perspective* (Springer Science, Business Media, 2003).
[34]P. E. Blochl, Phys. Rev. B **50**, 17953 (1994).
[35]G. Kresse and J. Hafner, Phys. Rev. B **47**, 558 (1993).
[36]G. Kresse and J. Hafner, Phys. Rev. B **49**, 14251 (1994).
[37]H. Jonsson, G. Mills, and K. W. Jacobsen, "Nudged elastic band method for finding minimum energy paths of transitions," in *Classical and Quantum Dynamics in Condensed Phase Simulations*, edited by B. J. Berne, G. Cicotti, and D. F. Coker (World Scientific, Singapore, 1998), pp. 385–404.
[38]G. Mills, H. Jonsson, and G. K. Schenter, Surf. Sci. **324**, 305 (1995).
[39]R. A. Olsen, G. J. Kroes, G. Henkelman, A. Arnaldsson, and H. Jónsson, J. Chem. Phys. **121**, 9776–9792 (2004).
[40]G. Henkelman, B. P. Uberuaga, and H. J. Jónsson, J. Chem. Phys. **113**, 9901 (2000).
[41]A. Azcatl, S. McDonnell, S. KC, X. Peng, H. Dong, X. Qin, R. Addou, G. I. Mordi, N. Lu, J. Kim, M. J. Kim, K. Cho, and R. M. Wallace, Appl. Phys. Lett. **104**(11), 111601 (2014).
[42]S. KC, H. Dong, W. Wang, R. C. Longo, K. Xiong, R. M. Wallace, and K. Cho, J. Appl. Phys. **115**, 023703 (2014).
[43]K. Xiong, W. Wang, D. M. Zhernokletov, S. KC, R. C. Longo, R. M. Wallace, and K. Cho, Appl. Phys. Lett. **102**, 022901 (2013).
[44]*CRC Handbook of Chemistry and Physics*, 84th ed., edited by D. R. Lide (CRC Press, Boca Raton, FL, 2003).
[45]D. Liu, Y. Guo, L. Fang, and J. Robertson, Appl. Phys. Lett. **103**, 183113 (2013).

[46]S. KC, R. C. Longo, R. Addou, R. M. Wallace, and K. Cho, Nanotechnology **25**(37), 375703 (2014).
[47]Y. Shi, B. Guo, S. A. Corr, Q. Shi, Y. S. Hu, K. R. Heier, L. Chen, R. Seshadri, and G. D. Stucky, Nano Lett. **9**(12), 4215–4220 (2009).
[48]D. O. Scanlon, G. W. Watson, D. J. Payne, G. R. Atkinson, R. G. Egdell, and D. R. Law, J. Phys. Chem. C **114**, 4636–4645 (2010).
[49]G. Lee, B. Lee, J. Kim, and K. Cho, J. Phys. Chem. C **113**(32), 14225–14229 (2009).
[50]D. R. Dreyer, S. Park, C. W. Bielawski, and R. S. Ruoff, Chem. Soc. Rev. **39**, 228–240 (2010).
[51]B. Radisavljevic and A. Kis, Nature Mater. **12**, 815–820 (2013).
[52]S. McDonnell, B. Brennan, A. Azcatl, N. Lu, H. Dong, C. Buie, J. Kim, C. L. Hinkle, M. J. Kim, and R. M. Wallace, ACS Nano **7**(11), 10354 (2013).
[53]A. Pasquarello, M. S. Hybertsen, and R. Car, Nature **396**, 58 (1998).
[54]F. Rochet *et al*., Adv. Phys. **35**, 237–274 (1986).
[55]A. M. Stoneham, C. R. M. Grovenor, and A. Cerezo, Philos. Mag. B **55**, 201–210 (1987).
[56]N. F. Mott, S. Rigo, F. Rochet, and A. M. Stoneham, Philos. Mag. B **60**, 189–212 (1989).
[57]P. Fahey, P. B. Grifrn, and J. D. Plummer, Rev. Mod. Phys. **61**, 289–384 (1989).
[58]C. Hinkle, M. Milojevic, A. Sonnet, H. Kim, J. Kim, E. M. Vogel, and R. M. Wallace, ECS Trans. **19**(5), 387–403 (2009).
[59]S. KC, W. Wang, H. Dong, K. Xiong, R. C. Longo, R. M. Wallace, and K. Cho, J. Appl. Phys. **113**, 103705 (2013).
[60]R. V. Galatage, D. M. Zhernokletov, H. Dong, B. Brennan, C. L. Hinkle, R. M. Wallace, and E. M. Vogel, J. Appl. Phys. **116**, 014504 (2014).
[61]C. Ataca and S. Ciraci, J. Phys. Chem. C **115**(27), 13303–13311 (2011).
[62]W. Chen, E. J. G. Santos, W. Zhu, E. Kaxiras, and Z. Zhang, Nano Lett. **13**, 509–514 (2013).